

Seasonal cycle of desert aerosols in West Africa : analysis of the coastal transition with passive and active sensors

Habib Senghor ¹, Éric Machu ^{1,2}, Frédéric Hourdin ³, and Amadou Thierno Gaye ¹

¹Laboratoire de Physique de l'Atmosphère et de l'Océan Siméon-Fongang (LPAO-SF), École Supérieure Polytechnique (ESP) de l'Université Cheikh Anta Diop de Dakar (UCAD), Sénégal.

²Laboratoire d'Océanographie Physique et Spatiale (LOPS), IUEM, Université Brest, CNRS, IRD, Ifremer, Brest, France.

³Laboratoire de Météorologie Dynamique (LMD), CNRS/IPSL/UMPC, Paris, France.

Correspondence to: H. Senghor (habib.senghor@ird.fr)

1 **Abstract.** The impact of desert aerosols on climate, atmospheric processes and the environment is still debated in the scientific
2 community. The extent of their influence remains to be determined and particularly requires a better understanding of the
3 variability of their distribution. In this work, we studied the variability of these aerosols in West Africa using different types of
4 satellite observations. SeaWiFS (Sea-Viewing Wide Field-of-View Sensor) and OMI (Ozone Monitoring Instrument) data have
5 been used to characterize the spatial distribution of mineral aerosols from their optical and physical properties over the period
6 2005-2010. In particular, we focused on the variability of the transition between the West African continent and the Eastern
7 Atlantic Ocean. Data provided by the Lidar scrolling CALIOP (Cloud-Aerosol Lidar with Orthogonal Polarization) onboard
8 the satellite CALIPSO (Cloud Aerosol Lidar and Infrared Pathfinder Satellite Observations) for the period 2007-2013 were then
9 used to assess the seasonal variability of the vertical distribution of desert aerosols. We first obtained a good representation of
10 Aerosol Optical Depth (AOD) and Single Scattering Albedo (SSA) by satellites SeaWiFS and OMI respectively in comparison
11 with AERONET estimates, both above the continent and the ocean. Dust occurrence frequency is higher in spring and boreal
12 summer. In spring, the highest occurrences are located between the surface and 3 km above sea level, while in summer the
13 highest occurrences are between 2 and 5 km altitude. The vertical distribution given by CALIOP also highlights an abrupt
14 change at the coast from spring to fall with a layer of desert aerosols confined in an atmospheric layer uplifted from the
15 surface of the ocean. This uplift of the aerosol layer above the ocean contrasts with the winter season during which mineral
16 aerosols are confined in the atmospheric boundary layer. Radiosondes at Dakar Weather Station (17.5°W, 14.74°N) provide
17 basic thermodynamic variables which partially give causal relationship between the layering of the atmospheric circulation over
18 West Africa and their aerosol contents throughout the year. A SSA increase is observed in winter and spring at the transition
19 between the continent and the ocean. The analysis of mean NCEP (National Center for Environmental Prediction) winds at
20 925 hPa between 2000 and 2012 suggest a significant contribution of coastal sand sources from Mauritania in winter which
21 would increase SSA over the ocean.

22 1 Introduction

23 The Sahara is the largest source of mineral aerosols in the world, with a contribution of almost 40% compared to the overall
24 emissions from natural sources (Ramanathan et al., 2001; Tanaka et al., 2005). The mineral dust aerosols emitted from the
25 Sahara desert can be transported over long distances in the atmosphere and can be detected as far as Americas (Prospero et al.,
26 1981; Swap et al., 1992; Formenti et al., 2001; Kaufman et al., 2005; Ansmann et al., 2009; Ben-Ami et al., 2010), Mediter-
27 ranean region (Bergametti et al., 1989; Moulin, 1997; Ansmann et al., 2003) and Asia (Ganor and Mamane, 1982; Israelevich
28 et al., 2003; Ganor et al., 2010). But here, the study of dust transport focuses on the main corridor of their transport Westward
29 of Africa (Formenti et al., 2001). They play a very important role on the climate and the various processes involved in the
30 climate system (Kaufman et al., 2005; Teller and Levin, 2006; Stith et al., 2009) through their direct impact in the visibility, in
31 the infrared (Sokolik and Toon, 1999) or the earth radiation budget (Andreae et al., 1996; Solomon, 2007) which is still poorly
32 known. The difficulty of understanding the impact of aerosols on the Earth's radiation balance is due to the large spatial and
33 temporal variability of their concentration and composition in the atmosphere. The mineral particles suspended in the atmo-
34 sphere come from different sources and have a nature similar to the nature of the soil from which they arise (Claquin et al.,
35 1999; Formenti et al., 2008) with a broad spectrum of particle sizes ranging between $0.01 \mu\text{m}$ and $300 \mu\text{m}$ (Wagener, 2008;
36 Ryder et al., 2013). Their impact on the marine ecosystem and particularly on oceanic primary production (Duce and Tindale,
37 1991; Baker et al., 2003; Mills et al., 2004; Jickells et al., 2005; Mahowald et al., 2009) remains still uncertain and difficult
38 to assess because of the composition of these particles and of physico-chemical processes affecting them (e.g., Friese et al.,
39 2016). Mineral dust deposition also have a negative impact on human health and are responsible for meningitis epidemics or
40 cardiac diseases (Thomson et al., 2006; Martiny and Chiapello, 2013; Diokhane et al., 2016; Prospero et al., 2005; Griffin,
41 2007).

42 Although the transport of mineral dust across the Atlantic Ocean started to be investigated in the 1960s, it started to be studied
43 from satellite observations since 1970s (Kaufman et al., 2005; Taghavi and Asadi, 2008). Passive sensors have the advantage
44 of providing daily data on the state of the atmosphere with good spatial and temporal coverage. The satellite products have
45 improved our knowledge of the source regions and dust transport pathways in recent years (Engelstaedter et al., 2006; Schep-
46 anski et al., 2007, 2009b, 2012). However, studies of their spatial and temporal variability are mainly based on indices such
47 as the Aerosol Optical Depth (AOD) or the Aerosol Index (AI) which provide vertically integrated information on the atmo-
48 spheric aerosol contents (passive space derived observations: Cakmur et al. (2001); Chiapello and Moulin (2002); Kaufman
49 et al. (2005); Engelstaedter et al. (2006); Schepanski et al. (2009b)). Moreover AOD estimated by satellite integrates the con-
50 tribution of every kind of particles and this latter estimation also depends on the altitude at which aerosols are located. Based
51 on perturbations induced by the Rayleigh scattering in the detection of absorbing aerosols, Chiapello et al. (1999) showed that
52 TOMS AI is more sensitive to aerosols present at high altitude than at low altitude. In other words the signal changes with the
53 height of the aerosol plume for a given aerosol content.

54 Recently, the vertical structure of the Saharan Air Layer (SAL) has been analyzed from CALIPSO satellite observations. The
55 vertical discontinuity of dust layers between land and ocean strongly impacts the atmospheric deposition rates of mineral mat-

56 ters (Schepanski et al., 2009a) and dust concentration at the oceanic surface which has important consequences on the primary
57 biological productivity of surface waters (Martin, 1992; Arístegui et al., 2009).
58 In boreal summer, SAL is characterized by hot, dry air, very dust-laden and is located between 10°N and 25°N (Dunion and
59 Marron, 2008; Tsamalis et al., 2013). This SAL is marked by very strong potential temperatures up to 40°C and a radon pres-
60 ence (radon-222) indicating the desert origin of air masses (Carlson and Prospero, 1972).
61 In winter, the SAL is characterized by the transport of dust containing chemical elements such as aluminum (Al), silicon (Si),
62 iron (Fe), titanium (Ti) and manganese (Mn) (e.g., Formenti et al., 2001; Ben-Ami et al., 2010) and is located between 5°N and
63 10°N (e.g., Tsamalis et al., 2013). Some of studies relating aerosols to their transport are generally a simple description of the
64 vertical distribution of aerosols in the SAL (Generoso et al., 2008; Liu et al., 2008; Ben-Ami et al., 2009; Braun, 2010; Yu et al.,
65 2010; Adams et al., 2012; Ridley et al., 2012; Yang et al., 2012) or a description of the seasonality of the SAL in connection
66 with large-scale dynamics (Liu et al., 2012; Tsamalis et al., 2013). However, the dust field campaigns, AMMA, SAMMUM-1
67 and 2, FENNEC or SALTRACE (see Table 1) of Weinzierl et al., (2016) carried out in West Africa and over the Atlantic Ocean
68 improved our understanding of dust-dynamics interactions. During SALTRACE, a linear depolarization ratio of particles and
69 a relative humidity threshold of 50% were used for differentiating different types of aerosol (Weinzierl et al., 2016). Authors
70 showed that sea salt aerosol were restricted to the lower layer superposed by biomass-dust mixtures. They also showed that the
71 altitude of the mineral dust layer decreased westward. The effects of small-scale dynamics and thermodynamics for controlling
72 the vertical structure of desert aerosols in coastal West Africa remain unknown, and efforts made in this direction are restricted
73 to very sporadic case studies (Gamo, 1996; Reid et al., 2002; Petzold et al., 2011).
74 In this study, in-situ and satellite observations are used to describe the seasonal time-scale of mineral dust distribution. We first
75 used complementary information, provided by SeaWiFS and OMI which deliver extensive (AOD) and intensive (SSA, AE)
76 parameters of desert aerosols, to analyse the spatial variability of the desert aerosol dust. Then we used CALIOP lidar on board
77 CALIPSO to investigate the vertical distribution of these desert aerosols.
78 We finally analyze meteorological data to explain the impact of the atmospheric variables on the seasonal cycle of the vertical
79 distribution of desert aerosols at the transition zone between the continent and the ocean. We conclude the present work by
80 summarizing all the results which are reflecting our common knowledge on mineral dust discrimination and spatio-temporal
81 distribution.

82 **2 Methodology and Data**

83 **2.1 AErosol RObotic NETwork (AERONET)**

84 We first used data of AOD from AERONET between January 2005 and December 2010. AERONET is a global network of in-
85 situ observations developed by the NASA Earth Observing System (NASA's EOS) (Dubovik et al., 2000). AERONET consists
86 of solar photometers Cimel providing measures of AOD every 15 minutes, refractive index and also allows inversions such as
87 particle size distribution of aerosols and single scattering albedo (SSA) at 440nm, 670nm, 870nm and 1020nm wavelengths
88 (Holben et al., 1998) with an accuracy of ± 0.01 (Slutsker and Kinne, 1999; Dubovik et al., 2000; Holben et al., 2001). This

89 uncertainty is inherent in the algorithm inversion used to retrieve aerosol characteristics. Some approximations are used in
90 the numerical inversion algorithm which produce errors named relative errors having a standard deviation of 0.01 (Dubovik
91 et al., 2000). AERONET's SSA are computed for favorable atmospheric conditions (AOD 440 nm > 0.4 and solar zenith angle
92 >45°) using an algorithm which performs almucantar inversions (Jethva et al., 2014). These data are used to validate remotely
93 sensed AOD and SSA measurements. AERONET is available under three different products: Level 1.0, 1.5 and 2.0. In this
94 study, we use Level 1.5 product for Cape Verde, due to a lack of sufficient Level 2 data, for this station and Level 2.0 for the
95 other stations. Concerning the temporal resolution of AERONET observations, we compute a “daily” mean based upon data
96 collected between 10am and 3pm in order to use observations collected during the same time window as satellite overpass. We
97 then use this 10am-3pm daily averages to compute monthly 10am-3pm AOD.

98 **2.2 Sea-viewing Wide Field-of-view Sensor (SeaWiFS)**

99 We then used DeepBlue-SeaWiFS monthly mean AOD at 550 nm and AE products derived from SeaWiFS developed by NASA
100 to study ocean color. SeaWiFS measures the solar radiation reflected at the top of the atmosphere in the wavelengths 412 nm,
101 443 nm, 490 nm, 510 nm, 555 nm, 670 nm, 765 nm and 865 nm. Satellite measurements carried out between October 1997 and
102 December 2010 (Jamet et al., 2004; Hsu et al., 2012) have a value of signal-to-noise and uncertainty of 2%-3% for the different
103 spectral bands (for details see Eplee et al. (2007); Franz et al. (2007); Eplee Jr et al. (2011)). In this paper, we use the Level 3
104 version 4 products (Bettenhausen and Team, 2013) for years 2005 to 2010. The SeaWiFS AOD provided at 550 nm is available
105 both over the land and over the ocean (Hsu et al., 2004; Sayer et al., 2012). The products used here are land-ocean estimates
106 generated and made available to the scientific community by NASA (Wang et al., 2000). Regarding the contribution of the
107 aerosols types in the AOD, the studies of Dubovik et al. (2002), Schepanski et al. (2009b) or Tegen et al. (2013) suggested that
108 the coarse mode fraction of mineral dust dominates the atmospheric mixture when AE values, associated with AOD values
109 greater than or equal to 0.3, are below 0.7. Here, we consider aerosols optical thickness larger than 0.2 when the Ångström
110 Exponent is lower than 0.7 (figure 4) to monitor the evolution of coarse (upper and lower bounds respectively) and fine (lower
111 and upper bounds) modes of mineral aerosols.

112

113 **2.3 Ozone Monitoring Instrument (OMI)**

114 OMI is a passive sensor on board the Aura satellite launched on 15 July 2004 by NASA's EOS Aura space-craft which released
115 its first observations in October 2004. Like all satellites in the A-Train constellation, OMI scans the entire Earth in 14 to 15
116 orbits with a nadir ground pixel spatial resolution of $13 \times 24 \text{ km}^2$ (Jethva et al., 2014). In addition to the ozone content in the
117 atmosphere OMI provides information on aerosols, clouds, gases (NO₂, SO₂, HCHO, BrO, and OCIO) and irradiance in the ul-
118 traviolet (Levelt et al., 2006). We use Aura/OMI SSA at 500 nm taken from <https://ozoneaq.gsfc.nasa.gov/data/lance-browse/>,
119 the OMAERUV Level 3 Collection 003 aerosol product processed in March 2012 with a spatial resolution of $1^\circ \times 1^\circ$ to quantify
120 the scattering of the aerosol types with passive sensors. The OMAERUV algorithm assigns flag to each pixel which carries
121 information on the quality of the retrieval (Jethva et al., 2014).

122 The SSA represents the ratio (ranging between 0 and 1) of scattering coefficient to extinction coefficient and provides infor-
 123 mation about the absorbing properties of the aerosols. SSA of 0.9 indicates that 90% of the total extinction of solar light is
 124 caused by scattering and 10% by absorption effects (Jethva et al., 2014). This parameter depends on the wavelength, size and
 125 the complex refractive index of particles (Léon et al., 2009). The closer this value is to one the more desert aerosols dominate
 126 (Johnson et al., 2008; Léon et al., 2009; Ialongo et al., 2010; Malavelle, 2011).
 127 OMI data were interpolated on the grid of SeaWiFS data to superimpose the products (AOD and SSA).

128 2.4 Cloud Aerosol Lidar and Infrared Pathfinder Satellite Observations (CALIPSO)

129 The first polarization lidar in space so-called CALIPSO is a sun-synchronous satellite developed by NASA as part of the Earth
 130 System Science Pathfinder program (ESSP) and launched on April 28, 2006 (Winker et al., 2007; Hunt et al., 2009) in order
 131 to provide a global coverage of the vertical distribution of the properties of clouds and aerosols (Winker, 2003). The CALIOP
 132 lidar (LIght Detection and Ranging) onboard CALIPSO acquires vertical profiles of the atmosphere at 30 m resolution in the
 133 lower layers (from the two orthogonal components that result from depolarization of a signal backscattered laser at 532 nm and
 134 vertical profiles of a total laser at 1064 nm signal backscattered at nadir). The final level-2 product is reduced to a uniform res-
 135 olution calculated from averaging and/or interpolating different resolutions for generating intermediate products (Winker et al.,
 136 2006). We use the Vertical Feature Mask (VFM; stage 1 Version 3) for which the processing algorithm is described in CALIOP
 137 Algorithm Theoretical Basis, Part 3: Scene Algorithms Classification (Liu et al., 2005). VFM allows to separate aerosols from
 138 clouds but also the desert aerosols from other types of aerosols (Omar et al., 2009). This methodology of discrimination by
 139 CALIOP of aerosol types gives results close to another method of distinction between mineral dust made from inversions (SSA
 140 and AE) of AERONET level 2 products (Mielonen et al., 2009). The mix of layers of desert aerosol and other types of aerosols
 141 (i.e. biomass burning) is very rare (Chou et al., 2008; Heese and Wiegner, 2008) in our region of interest. During the dry season,
 142 mineral aerosols are observed in the atmospheric surface layer ranging 0.5 to 1 km while the aerosol emitted through biomass
 143 burning are carried to higher levels up to 5 km altitude (Cavalieri et al., 2010). Nevertheless, classification errors are possible
 144 for low values of the Mineral Dust Occurrence Frequency (MDOF) and at frontal zones between layers of different substances
 145 (Adams et al., 2012). For this reason we only consider here the values of MDOF above 10%. Our method for determining the
 146 mineral dust by a calculation of the MDOF is equivalent to Adams et al. (2012) and follows the equation:

147

$$148 \quad p(x, y, z) = \frac{\sum_{n=0}^N p(x+n, y, z)}{\sum_{n=0}^N s(x+n, y, z)} \quad \forall \quad x, y, z \quad (1)$$

149

150

151 where p is the frequency of occurrence of dust at a grid point, s the total number of valid satellite passing the same grid
152 point and N the total number of grid points. The Occurrences in the longitude (x) are summed and normalized by the total
153 valid satellite passes in a given longitudinal range (35°W - 20°E). Data were gridded with a near-uniform horizontal resolution
154 of $0.5^{\circ} \times 0.5^{\circ}$ and a vertical resolution of 30 m for 290 vertical levels between 0.5 and 8.2 km above sea level. The CALIOP
155 lidar on CALIPSO (also in the A-train) has a 90 m instantaneous footprint which is smeared to 333 m in the along track
156 direction by orbital motion over the lidar pulse duration. All satellites of the A-train constellation, such as CALIPSO, fly in
157 a sun-synchronous orbit with a 16 days coverage cycle consisting of 233 orbits separated by 1.54 degrees longitude or about
158 172 km at the equator. Each satellite completes 14.55 orbits per day with a separation of 24.7 degrees longitude between each
159 successive orbit at the equator. These CALIPSO orbits are controlled to cover the same ground with cross-track errors of less
160 than ± 10 km (Winker et al., 2007). This drastically reduces the spatial coverage of the satellite. Consequently, we use a mesh
161 of 0.5° longitude to cover the area between 10°W - 24°W and 12°N - 21°N . The choice of this band of latitude is driven by one
162 of the objectives of the paper which is to study the transition of aerosol distribution between the continent and the ocean. Dust
163 occurrences are averaged over latitudes 12°N to 21°N and are then smoothed over 30 points longitudinal running mean and 50
164 points vertical running mean.

165 **3 Results**

166 **3.1 Horizontal dust distribution**

167 SeaWiFS AOD (estimated at wavelength 550 nm) represents an average value of the optical Depth of the atmosphere. It has first
168 been compared to the monthly AOD given by AERONET photometers (given at the wavelength 675 nm and interpolated at 550
169 nm) by calculating the correlation between the two measurements at different selected stations (Fig. 1). Our choice focused
170 on the stations Banizoumbou (2.665°E - 13.541°N), Agoufou (1.479°W - 15.345°N), M'bour (16.959°W - 14.394°N) and Capo
171 Verde (22.935°W - 16.733°N) to assess the quality of satellite information obtained across the land-ocean continuum. A very
172 good correlation is calculated between SeaWiFS and in-situ measurement given by the photometer at Banizoumbou ($R=0.97$;
173 Fig. 1a). The photometer Cimel at Agoufou (Mali) also shows a very good correlation with SeaWiFS ($R=0.87$; Fig. 1b). The
174 correlation between the two measures is equal to 0.81 at the shore in M'bour (Fig. 1c). It is close to the one in Capo Verde
175 ($R=0.83$; Fig. 1d). All these correlation values of AOD are significant at 95% using a student statistical test. The regression
176 for M'bour site is not as good as for the other sites. This site is located at the shore at the interface between land and sea and
177 the satellite algorithm retrieval is not the same over the land and over the ocean. We also studied the structure of the cloud of
178 points between the two datasets to assess the quality of the satellite measurements as a function of the aerosol concentration.
179 The regression line obtained by the least squares method shows a linear relationship between satellite and in-situ monthly mean
180 measurements of AOD at the selected stations.

181 The horizontal transport of desert aerosols can be followed by considering the key and complementary parameters that distin-
182 guish them. To better characterize the desert aerosols, we combined AOD (SeaWiFS) with SSA (OMI) to specify the contribu-
183 tion of the latter compared to other types of aerosols in the atmosphere. A threshold of 0.90 in monthly averaged SSA is used

184 to define regions dominated by desert aerosols. This value is chosen in agreement with the threshold value given in previous
185 studies (Léon et al., 2009; Malavelle, 2011; Jethva et al., 2014). This method allowed us to define the Sahelo-Saharan region
186 as the one which is the most influenced by dust plumes composed of desert aerosols throughout the year (between 12°N and
187 21°N; Fig. 3).

188 The comparison of the daily SSA of Aura/OMI versus AERONET is achieved to validate satellite SSA which provides a better
189 spatio-temporal coverage of our region of interest. OMI SSA retrievals are taken between 10am and 3pm time range which
190 cover AERONET measurements. As emphasized by Jethva et al. (2014), this comparison is done at the original wavelengths
191 of each independent measurement (388 nm for OMI and 440 nm for AERONET) in order to avoid uncertainties induced by the
192 interpolation at other wavelengths. Good correlations are retrieved between the two datasets at the different ground stations in
193 West Africa for the period 2005-2010 within root mean square (RMS) difference of 0.03 in the selected region (Fig. 2). Glob-
194 ally, the OMAERUV SSA is well correlated with ground measurements. The correlation at all selected sites for this study is
195 significant. The agreement between the two inversions is better over the continent (Banizoumbou station, $r=0.47$ and Agoufou
196 station: $r=0.50$) and at the shore of West Africa (M'bour station: $r=0.66$) than over the ocean (Capo Verde station: $r=0.30$).
197 The discrepancy between the AERONET SSA retrievals over continent (Banizoumbou and Agoufou) and at the shore of West
198 Africa (M'bour) was already found by Johnson and Osborne (2011) during GERBILS campaign over West Africa. These au-
199 thors suggested that a lack of sampling may affect the results. Their results are in agreement with our results which show 449
200 retrievals in Banizoumbou against 178 retrievals in M'bour site.

201 Figure 3 shows a seasonal distribution of the AOD which superimposed onto SSA in West Africa region. Both, large AOD
202 and strong SSA indicate that mineral dust is the dominant component of aerosols in the atmosphere. In winter, the main dust
203 source in West Africa, the Bodélé depression, is showed in Figure 3a with AOD larger than 0.5 and SSA larger than 0.9 around
204 17°N-18°E. This most persistent dust hot spot is activated all along the year and provides a maximum dust emission in spring
205 (Fig. 3b), in agreement with Engelstaedter and Washington (2007). In summer, the intense surface heating from solar radiation
206 (Heat Low) induces the development of a near-surface thermal low pressure system over northern Mali, southern Algeria, and
207 eastern Mauritania (Lavaysse et al., 2009; Messenger et al., 2010) and controls the dry convective processes which contribute to
208 about 35% of the global dust budget (Engelstaedter and Washington, 2007). Over Northwestward Sahara region (Fig. 3c), the
209 AOD is larger than 0.5 and SSA is stronger than 0.9, both variables indicate the main hot spot of mineral dust source in West
210 Africa in summer which has already been shown by Engelstaedter and Washington (2007).

211 Figures 3 and 4 show that horizontal monthly average of AOD is stronger above the continent than over the ocean throughout
212 the year. The weakest AOD is given for winter months (DJF for December-January-February) with a mean value of $0.33 \pm$
213 0.07 (standard deviation). At this season, the SSA values are higher in the northeast tropical Atlantic than on the West African
214 continent with a SSA maximum reaching 0.95. This indicates a stronger contribution of dust over the ocean than over the con-
215 tinent in the latitude range 12°N-21°N. Note that sources of dust aerosols are also indicated by high SSA values north of 21°N.
216 The air masses advection in the lower atmosphere (925 hPa) follows a NorthEast-SouthWest direction in winter (Fig. 6a), dust
217 coming from the NorthWest of Mauritania is partially seen over the continent (in AOD and SSA) and its main signature should
218 be seen over the ocean. In spring (MAM for March-April-May), the increase of the monthly mean AOD compared to winter is

219 indicated by a stronger mean value (0.50 ± 0.08). The mean optical depth indicates that the dust sources are becoming more
220 active with an atmosphere more charged than in winter. The coarse mode dominates in the mixed atmosphere boundary layer
221 over the continent with lower values of AE less than 0.7 (not shown). Nevertheless, the reflectance properties of aerosols (given
222 by the SSA) is higher over the ocean than over the continent and vary weakly compared to winter.
223 In summer (JJA for June-July-August), the maximum mean AOD is 0.52 ± 0.05 . AOD values are associated with higher SSA
224 above 0.96. It indicates that aerosols are clearly dominated by desert dust in boreal summer. At this season, important quantity
225 of dust can be lifted up and vertically transported in the upper atmosphere by convective systems and near-surface convergence
226 (Engelstaedter and Washington, 2007).
227 In autumn (SON for September-October-November), the monthly mean AOD is 0.34 ± 0.05 . AOD is decreased compared to
228 spring but the SSA values are much higher than in spring despite the fact that uplift occurrences are larger in spring than in fall
229 in West Africa (Marticorena et al., 2010; Diokhane et al., 2016).
230 Changes of AOD and SSA are seen at the transition between the continent and the ocean (Fig. 4). Understanding these changes
231 requires a thorough analysis of the vertical distribution of dust during transportation from east to west in North Africa.

232 **3.2 Vertical dust distribution**

233 The vertical distribution of desert aerosol indicates a strong presence of dust concentrations between the surface and 6 km in
234 agreement with the results of Léon et al. (2009) who studied the vertical distribution of dust in the North-East Tropical Atlantic
235 (Fig. 5).

236 In DJF, desert aerosols are mainly concentrated in the atmospheric boundary layer (ABL) between the surface and 2 km
237 (Fig. 5a) both over the continent and the ocean. At this season, we also noted a homogeneous dust aerosol transition between
238 Western Africa and the Eastern part of the Atlantic Ocean.

239 In MAM, there is an elevation of the SAL with a maximum altitude of 5 km on the continent and between 4 and 5 km above
240 the ocean (Fig. 5b). The MDOF over 50% above the continent shows that dust emissions are much greater than in winter. The
241 ABL is developed vertically to reach up to 5 km of altitude. It results in an atmospheric layer well mixed between the surface
242 and 5 km of altitude above the continent (10°W - 15°W). Above the Ocean we see a detachment of the SAL from the ocean
243 surface which occurs at the coast (around 18°W).

244 JJA is the busiest season of the year in terms of dust rising in the northern hemisphere of Africa. It is characterized by the de-
245 velopment of density currents that intensify the mobilization of terrigenous aerosols (e.g., Bou Karam et al., 2008; Schepanski
246 et al., 2009b, Fig. 5c). Unlike DJF, we note a clear separation of the dust layer above the Eastern Atlantic Ocean where dusts
247 are confined between 1 and 6 km altitude.

248 In SON, dust emissions decrease in intensity compared to JJA but the detachment from the surface of the ocean remains clear
249 at the coast although less marked than in JJA (Fig. 5d). According to Adams et al. (2012), the heart of the SAL is located about
250 5 km above sea level in SON, whereas Liu et al. (2012) shows a maximum altitude of 4 km.

252 **4.1 Seasonal variability**

253 The desert aerosols in the band of latitude 12°N - 21°N are mainly emitted in the Saharan and Sahelian regions. Emissions and
254 transport processes are mainly controlled by meteorological variables (Brooks and Legrand, 2000; Joseph, 1999).

255 Schepanski et al. (2009b) found that over the Sahara sources of dust emissions are less active in winter than during summer
256 season. The southward migration of the ITCZ and the subsiding branch of the Hadley cell over the dry convection can also
257 prevents the deep vertical distribution of aerosols in north Africa (Lavaysse et al., 2009). The maximum altitude of this distri-
258 bution is 3 km above the continent and 2 km at the West African coast in agreement with the studies of Léon et al. (2009) and
259 Vuolo et al. (2009). Compared to other seasons, DJF show an important role played by the shallower atmospheric layers on
260 the dust transported from source regions located in the Northwestern part of Mauritania and more generally in the West African
261 coastal region (Fig. 6a). This high occurrence is shown by the inter-seasonal variability derived from NCEP Reanalysis. Figure
262 6 highlights that the Northwest region of Mauritania has the highest standard deviation of horizontal wind intensity between
263 18°N - 24°N and that wind is very intense in winter compared to the other seasons (Fig. 6a). Hence this region represents an
264 important sand source in winter as mentioned by previous studies (Bertrand et al., 1979; Ozer, 2000; Tulet et al., 2008; Laurent
265 et al., 2008; Mokhtari, 2012; Hourdin et al., 2015).

266 Unlike winter, as showed in Figure 5c, dust are concentrated between the higher layers of the ABL, from one to 5-6 km (Gamo,
267 1996), in response to intense convective mechanisms that are more common in the region at this season (Cuesta et al., 2009).
268 Indeed, the summer solar heating drives the development of the Saharan boundary layer which reaches up to 6 km while the
269 convergence of hot dry air (Harmattan) from the Sahara with fresh moist air (monsoon) from the ocean generates intense con-
270 vective cells which are responsible for the suspension of large amounts of dust which will be distributed in the ABL. Transport
271 is also growing between 3 and 4 km above the ocean with a MDOF greater than 70%, i.e. more than 30% higher than that
272 observed in DJF. This sharp increase of MDOF from DJF to JJA is in agreement with the results of Schepanski et al. (2009b)
273 who estimated an increase of more than 20% of the activity of dust sources in summer compared to winter in West Africa in the
274 observations of Meteosat Second Generation (MSG) Spinning Enhanced Visible and Infrared Imager (SEVIRI). In summer,
275 atmospheric dynamics raise large dust particles that are settling down much closer to the source regions than the rest of the
276 year (Shao, 2000). However, their reflectivity of solar radiation becomes larger and reaches a maximum value indicated by a
277 SSA of 0.97 (Fig. 4c).

278 In autumn, SSA values are comparable to spring values but these high values are not due to high reflectance of desert aerosols
279 like in spring because the southern migration of the Inter-Tropical Convergence Zone (ITCZ) reduces the activity of convective
280 systems and causes a reduction of dust emissions shown by a decreasing of the AOD (Fig. 4d). These high SSA values can be
281 attributed to atmospheric conditions seen through the relative humidity which is much higher than in spring (Fig. 7d). Indeed,
282 OMI measures the atmospheric properties of the aerosols which are known to be hygroscopic (Jethva et al., 2014).

283 4.2 Continent-Ocean transition

284 To better understand the factors responsible for the high variability of the vertical transition of desert aerosols from the con-
285 tinent to the ocean, we placed ourselves at a coastal point (Dakar) to study the variation of meteorological variables and their
286 potential influence on the distribution of aerosols. Seasonality of vertical distributions of winds, relative humidity and potential
287 temperature from radiosounding conducted at the weather station (GOOY) of Dakar (at West African shore) are shown in
288 Figure 7.

289 In DJF, continental winds are very strong at the near-surface with a maximum of 25 m/s at 500 m (Fig. 7a). The north-east
290 direction of the winds in the first thousand meters explains the homogeneity of the vertical distribution of dust from the con-
291 tinent towards the ocean. This north-east wind applies to all West Africa at the surface (Fig 6a). Their intensity also explain
292 the strong values of MDOF (up to 50%) observed by CALIOP in wintertime above the continent. Between 1 and 2 km height,
293 winds weaken and change direction (south to south-east) while MDOF observed by satellite decreases (Fig. 5a). Between 2
294 and 5 km height, the winds turn to the southwest and west. These dust-depleted air masses of oceanic origin are wetter than
295 from the land, and limit the development of the ABL. The air masses of continental origin are located between the surface and
296 2000 m height (Fig. 7a). In Figure. 7a, the relative humidity is around 20% (between 500 and 2000 m) and it corresponds to a
297 very dry air mass of Saharan origin. Between 2 and 5 km the potential temperature indicates a stable atmospheric layer. This
298 season is associated with an intermediate AOD value which decreases from 15°E to 10°W. SSA reflects mineral dust properties
299 across its westward transportation (>0.9) but is higher by 0.2 over the ocean than the continent. We believe it could reflect
300 the transport of dust emitted along the coastline which is only partly taken into account in dust properties derived from the
301 continent.

302 Compared to the DJF situation, MAM near-surface winds (Fig. 7b) are still intense with a maximum of 25 m/s at 500 m height
303 and are from the east. They are associated with MDOF above 50% in the ABL around 14°W. Surface winds (Fig 6b) shows the
304 near-surface convergence of northward and southward flows along 16°N which is associated with a well-mixed distribution
305 of dust in the first 5 km of the atmosphere (Fig 5b) and higher AOD values than in winter (Fig 4). There is an inversion of
306 easterly winds between 1 and 3 km and a second southerly wind peak (15 m/s) appears between 3 and 4 km. It corresponds
307 to the dust layer (SAL) detected by CALIOP. The vertical profile of potential temperature indicates a stable thick layer, well
308 mixed between the surface and 3 km (Fig. 7b). Beyond this altitude there is a stable stratification of the atmosphere indicated
309 also by the potential temperature. Between 3 and 5 km height, the air masses coming from the South to the South-Southwest
310 are also of oceanic origin and their interaction with a more consistent amount of dust than in winter could explain the better
311 marked transition between the ocean and the continent in terms of SSA (increase) and AOD (decrease) for this season (Fig. 4b).
312 Indeed, in general, increasing the relative humidity is likely to increase the SSA and size hygroscopic aerosols with dry to wet
313 passage inducing a larger diameter even when humidity is below the saturation level (Hervo, 2013; Howell et al., 2006).

314 In JJA, surface winds (0-1 km) decrease and are from the West to the Southwest (West African Monsoon) (Fig. 7c). This
315 corresponds to lower values of MDOF (Fig. 5c) but to relative humidity values well above DJF or MAM (Fig. 7). Reid et al.
316 (2002) presented a conceptual model of Saharan dust transport in the middle troposphere describing an evolution of relative

317 humidity profile in agreement with the observations made in Dakar. These authors describe a moistening of the surface layers
318 due to monsoon flow which penetrates up to 1.5 km above this layer. Figure 6c shows deep intrusion of air masses coming
319 from the Gulf of Guinea which brings humidity into the continent. The dry convection taking place over the continent favors
320 the vertical transport of dust to high altitudes (Engelstaedter and Washington, 2007).

321 Between 2 and 6 km, winds are from the East and above 15 m/s. These wind velocity maxima reach 25 m/s in the range 3.5-5
322 km and are associated to the African Easterly Jet (AEJ) (Wu et al., 2009; Lafore et al., 2011). The co-localization of the AEJ
323 and the SAL between 2 and 5 km height (Fig. 5c and Fig. 7c) causes the westward SAL transport by AEJ in summer (Karyam-
324 pudi et al., 1999). These strong winds correspond to the layer of dust detected by satellite at this altitude (Fig. 5c). Above the
325 continent, the mesoscale features associated with the convergence between Harmattan and the West African Monsoon at the
326 ITCZ cause strong updrafts that allow lifting and transport of dust particles throughout the air column (Tulet et al., 2008). The
327 dynamics of the monsoon described by the conceptual scheme of mechanisms controlling the dust vertical redistribution in
328 Cuesta et al. (2009) explain the wide occurrence of dust found between 2 and 5 km rather than at the surface. During transport
329 from North Africa to the Atlantic Ocean, very large amounts of coarse dust (Fig. 4c) are deposited along the path with a rapid
330 change in the size distribution of aerosols near the west African coast (Ryder et al., 2013). The changes of the aerosol size and
331 properties will impact the climate system (Huneeus et al., 2011; Mahowald et al., 2014). McConnell et al. (2008) suggested that
332 the variation in the aerosol profiles over the ocean have an impact on the radiative effect, a statement confirmed by Highwood
333 et al. (2003) who showed that the radiative effect of mineral dust is correlated with the altitude of the dust layer.

334 The signing of the SAL is evidenced by relative dryness of the atmosphere (Dulac et al., 2001) between 1.5 and 5 km (Fig. 7c).
335 At this altitude, the vertical profile of potential temperature indicates Saharan origin of air masses with temperatures between
336 35°C and 45°C (Carlson and Prospero, 1972). The wind direction (east) given in Figure 7c between 1.5 and 5 km altitude con-
337 firms the origin of the Saharan air masses. The presence of dust in the SAL causes both warming and drying of the atmosphere
338 between 1.5 and 5 km and a cooling below this layer (Tulet et al., 2008).

339 In SON, winds are weak and from the East at the surface (Figs. 7d and 6d). Between 1 and 5 km, it is increasing but is less
340 intense than in JJA between 3 and 5 km and it is associated with a decrease of the MDOF (Fig. 5d). The moisture profile in
341 SON (Fig. 7d) is close to that of JJA, but has a more humid atmosphere in the layer between 1.5 and 5 km where maximum
342 relative humidity of the year occurs (60%; Fig. 7d). The analysis of the vertical distribution of thermodynamic variables like
343 relative humidity, potential temperature and wind measured at the Dakar weather station shows that the thermodynamical con-
344 ditions control the dust vertical distribution as well as the depth of the dust layer depending on the season. This analysis also
345 explains the unintuitive differences between spring, when the low values of SSA are associated with a strong AOD, and autumn
346 characterized by high values of SSA associated with low AOD values.

347 **5 Conclusions**

348 Studies of processes involved in the vertical distribution of aerosols at the transition between continent and ocean are very rare.
349 Here, we took advantage of a weather station ideally located on the main pathway of desert aerosols from Northern Africa

350 (Léon et al., 2009; Marticorena et al., 2010; Mortier et al., 2016) to explain the effect of meteorological variables on this transi-
351 tion in a region of primary importance worldwide. The interaction of air masses of oceanic origin with dust aerosols are crucial
352 for understanding their fate (e.g., Friese et al., 2016). This study constitutes the first attempt to relate the seasonal dynamic
353 of the atmosphere and the vertical distribution of dust aerosol in this region and provides the first dynamical explanation of a
354 counterintuitive deposition pattern over the Atlantic ocean. Indeed, it explains the role of the local atmospheric circulation in
355 driving a higher AOD and dust content in summer over west Africa in phase with dust deposition in Barbades islands but in
356 opposition with Cape Verde islands where deposition is more intense in winter (Chiapello et al., 1995).

357 We have studied the seasonal variability of the distribution of desert aerosols in West Africa (continental and oceanic) from
358 their optical and physical properties. First of all we have been able to show a good estimate of physical properties (AOD
359 and SSA) of aerosols by satellite when compared with AERONET ground measurements on the mainland, the coast and the
360 ocean. Space observations then allowed us to show the predominant presence of Saharan dust in the atmosphere north of 12°N
361 throughout the year and an additional significant contribution of sandy sources from the Mauritanian coast in winter. The
362 MDOF indicates a change in the vertical distribution of dust at the transition between the continent and the ocean, the largest
363 differences occurring in spring and summer seasons. In DJF, the ABL is shallow (~ 1 km) and strong winds from North-East
364 transport the dust in a dry atmosphere from the continent to the ocean continuously. This surface layer is superimposed by a
365 stable atmospheric layer which inhibits the vertical development of this surface layer rich in dust aerosols. The decrease from
366 east to west of the AOD requires material deposition during the transit. In summer dry convection located north of 10°N and
367 associated with structures that develop at the Inter-Tropical discontinuity (ITD) distribute dust up to 6 km height and create
368 a thicker AOD. Above 6 km altitude over the Saharan-Sahel areas, the vertical distribution of dust is blocked by the strong
369 subsiding branch of the Hadley cell (Lavaysse et al., 2009). In the lower layers, the westward oceanic moistly entries which are
370 opposite to the higher eastward winds generate very different distributions above the continent and the ocean. On the mainland,
371 the dust is dominated by coarse mode and have a homogeneous vertical distribution while above the ocean, lower layers are
372 poor in dust and are superimposed by the SAL which is highly enriched. The SSA remains constant at this transition. MAM
373 and SON represent transition periods. For the vertical dust distribution, MAM is being closer to the summer situation.

374 Future modeling experiments should bring further insights into ocean-atmosphere processes involved in explaining this transi-
375 tion and the dust deposition along this pathway. It also seems that a more tailored approach to ocean-atmosphere interactions
376 including higher frequencies of variability and notably the diurnal cycle is needed to make more apparent the role of local
377 circulation on the vertical distribution of aerosols in coastal areas.

378 *Acknowledgements.* We would like to thank the IRD-BMBF AWA project and the international joint laboratory ECLAIRS for supporting
379 and promoting our research activities. We thank the Institute of Research for Development for funding this PhD. We also thank ICARE for
380 the online availability of the CALIPSO aerosol products at <http://www.icare.univ-lille1.fr/archive>. NCEP Reanalysis data were found on-
381 line by the <http://www.esrl.noaa.gov/psd/data/gridded/data.ncep.reanalysis.pressure.html>, and the PIs and NASA for online AERONET data
382 set which can be obtained from <http://aeronet.gsfc.nasa.gov/>. OMI aerosol products were downloaded at [http://disc.gsfc.nasa.gov/gesNews/
383 giovanni_3_end_of_service?instance_id=omil2g&selectedMap=Blue%2520Marble&](http://disc.gsfc.nasa.gov/gesNews/giovanni_3_end_of_service?instance_id=omil2g&selectedMap=Blue%2520Marble&). We are very grateful to B. Marticorena and I. Chia-

384 pello for very fruitful discussions. We are finally very grateful to the two anonymous referees for very informative comments which have
385 greatly improved the quality of this study.

386 References

- 387 Adams, A. M., Prospero, J. M., and Zhang, C.: CALIPSO-derived three-dimensional structure of aerosol over the Atlantic Basin and adjacent
388 continents, *Journal of Climate*, 25, 6862–6879, 2012.
- 389 Alizadeh-Choobari, O., Sturman, A., and Zawar-Reza, P.: A global satellite view of the seasonal distribution of mineral dust and its correlation
390 with atmospheric circulation, *Dynamics of Atmospheres and Oceans*, 68, 20–34, 2014.
- 391 Andreae, M. O. et al.: Raising dust in the greenhouse, *Nature*, 380, 389–390, 1996.
- 392 Ansmann, A., Bösenberg, J., Chaikovskiy, A., Comerón, A., Eckhardt, S., Eixmann, R., Freudenthaler, V., Ginoux, P., Komguem, L., Linné,
393 H., et al.: Long-range transport of Saharan dust to northern Europe: The 11–16 October 2001 outbreak observed with EARLINET, *Journal*
394 *of Geophysical Research: Atmospheres*, 108, 2003.
- 395 Ansmann, A., Baars, H., Tesche, M., Müller, D., Althausen, D., Engelmann, R., Pauliquevis, T., and Artaxo, P.: Dust and smoke transport
396 from Africa to South America: Lidar profiling over Cape Verde and the Amazon rainforest, *Geophysical Research Letters*, 36, 2009.
- 397 Arístegui, J., Barton, E. D., Álvarez-Salgado, X. A., Santos, A. M. P., Figueiras, F. G., Kifani, S., Hernández-León, S., Mason, E., Machú,
398 E., and Demarcq, H.: Sub-regional ecosystem variability in the Canary Current upwelling, *Progress in Oceanography*, 83, 33–48, 2009.
- 399 Baker, A., Kelly, S., Biswas, K., Witt, M., and Jickells, T.: Atmospheric deposition of nutrients to the Atlantic Ocean, *Geophysical Research*
400 *Letters*, 30, 2003.
- 401 Ben-Ami, Y., Koren, I., and Altaratz, O.: Patterns of North African dust transport over the Atlantic: winter vs. summer, based on CALIPSO
402 first year data, *Atmospheric Chemistry and Physics*, 9, 7867–7875, 2009.
- 403 Ben-Ami, Y., Koren, I., Rudich, Y., Artaxo, P., Martin, S., and Andreae, M.: Transport of North African dust from the Bodélé depression to
404 the Amazon Basin: a case study, *Atmospheric Chemistry and Physics*, 10, 7533–7544, 2010.
- 405 Bergametti, G., DUTOT, A.-L., BUAT-MÉNARD, P., Losno, R., and Remoudaki, E.: Seasonal variability of the elemental composition of
406 atmospheric aerosol particles over the northwestern Mediterranean, *Tellus B*, 41, 353–361, 1989.
- 407 Bertrand, J., Cerf, A., and Domergue, J.: Repartition in space and time of dust haze south of the Sahara, *The Long-Range Transport of*
408 *Pollutants and its Relation to Gen. Circulation Including Stratospheric/Tropospheric Exchange Processes* p 409-415(SEE N 80-26888
409 17-45), 1979.
- 410 Bettenhausen, C. and Team, G. D. M.: Consistent Long-Term Aerosol Data Records over Land and Ocean from SeaWiFS, in: *Goddard Space*
411 *Flight Center Greenbelt, Maryland*, pp. 1–19, <http://disc.sci.gsfc.nasa.gov/dust/documentation/README.DeepBlueSeaWiFS.pdf>, 2013.
- 412 Bou Karam, D., Flamant, C., Knippertz, P., Reitebuch, O., Pelon, J., Chong, M., and Dabas, A.: Dust emissions over the Sahel associated with
413 the West African monsoon intertropical discontinuity region: A representative case-study, *Quarterly Journal of the Royal Meteorological*
414 *Society*, 134, 621–634, 2008.
- 415 Braun, S. A.: Reevaluating the role of the Saharan air layer in Atlantic tropical cyclogenesis and evolution, *Monthly Weather Review*, 138,
416 2007–2037, 2010.
- 417 Brooks, N. and Legrand, M.: Dust variability over northern Africa and rainfall in the Sahel, in: *Linking climate change to land surface*
418 *change*, pp. 1–25, Springer, 2000.
- 419 Cakmur, R. V., Miller, R. L., and Tegen, I.: A comparison of seasonal and interannual variability of soil dust aerosols over the Atlantic Ocean
420 as inferred by the TOMS AI and AVHRR AOT retrievals, *Journal of Geophysical Research: Atmospheres*, 106, 18 287–18 303, 2001.
- 421 Carlson, T. N. and Prospero, J. M.: The large-scale movement of Saharan air outbreaks over the northern equatorial Atlantic, *Journal of*
422 *applied meteorology*, 11, 283–297, 1972.

423 Cavalieri, O., Cairo, F., Fierli, F., Donfrancesco, G. D., Snels, M., Viterbini, M., Cardillo, F., Chatenet, B., Formenti, P., Marticorena, B.,
424 et al.: Variability of aerosol vertical distribution in the Sahel, *Atmospheric Chemistry and Physics*, 10, 12 005–12 023, 2010.

425 Chiapello, I. and Moulin, C.: TOMS and METEOSAT satellite records of the variability of Saharan dust transport over the Atlantic during
426 the last two decades (1979–1997), *Geophysical Research Letters*, 29, 2002.

427 Chiapello, I., Bergametti, G., Gomes, L., Chatenet, B., Dulac, F., Pimenta, J., and Santos Soares, E.: An additional low layer transport of
428 Sahelian and Saharan dust over the north-eastern tropical Atlantic, *Geophysical Research Letters*, 22, 3191–3194, 1995.

429 Chiapello, I., Prospero, J., Herman, J., and Hsu, N.: Detection of mineral dust over the North Atlantic Ocean and Africa with the Nimbus 7
430 TOMS, *Journal of Geophysical Research: Atmospheres*, 104, 9277–9291, 1999.

431 Chou, C., Formenti, P., Maille, M., Ausset, P., Helas, G., Osborne, S., and Harrison, M.: Size distribution, shape and composition of dust
432 aerosols collected during the AMMA SOP0 field campaign in the northeast of Niger, January 2006, *J. Geophys. Res.*, 113, D00C10, 2008.

433 Claquin, T., Schulz, M., and Balkanski, Y.: Modeling the mineralogy of atmospheric dust sources, *Journal of Geophysical Research: Atmo-*
434 *spheres*, 104, 22 243–22 256, 1999.

435 Cuesta, J., Marsham, J. H., Parker, D. J., and Flamant, C.: Dynamical mechanisms controlling the vertical redistribution of dust and the
436 thermodynamic structure of the West Saharan atmospheric boundary layer during summer, *Atmospheric Science Letters*, 10, 34–42, 2009.

437 Diokhane, A. M., Jenkins, G. S., Manga, N., Drame, M. S., and Mbodji, B.: Linkages between observed, modeled Saharan dust loading and
438 meningitis in Senegal during 2012 and 2013, *International journal of biometeorology*, 60, 557–575, 2016.

439 Dubovik, O., Smirnov, A., Holben, B., King, M., Kaufman, Y., Eck, T., and Slutsker, I.: Accuracy assessments of aerosol optical properties re-
440 trieved from Aerosol Robotic Network (AERONET) Sun and sky radiance measurements, *Journal of Geophysical Research: Atmospheres*,
441 105, 9791–9806, 2000.

442 Dubovik, O., Holben, B., Eck, T. F., Smirnov, A., Kaufman, Y. J., King, M. D., Tanré, D., and Slutsker, I.: Variability of absorption and
443 optical properties of key aerosol types observed in worldwide locations, *Journal of the atmospheric sciences*, 59, 590–608, 2002.

444 Duce, R. A. and Tindale, N. W.: Atmospheric transport of iron and its deposition in the ocean, *Limnology and Oceanography*, 36, 1715–1726,
445 1991.

446 Dulac, F., Chazette, P., Gomes, L., Chatenet, B., Berger, H., and Dos Santos, J. V.: A method for aerosol profiling in the lower troposphere
447 with coupled scatter and meteorological rawinsondes and first data from the tropical Atlantic off Sahara, *Journal of aerosol science*, 32,
448 1069–1086, 2001.

449 Dunion, J. P. and Marron, C. S.: A reexamination of the Jordan mean tropical sounding based on awareness of the Saharan air layer: Results
450 from 2002, *Journal of Climate*, 21, 5242–5253, 2008.

451 Engelstaedter, S. and Washington, R.: Atmospheric controls on the annual cycle of North African dust, *Journal of Geophysical Research:*
452 *Atmospheres*, 112, 2007.

453 Engelstaedter, S., Tegen, I., and Washington, R.: North African dust emissions and transport, *Earth-Science Reviews*, 79, 73–100, 2006.

454 Eplee, R. E., Patt, F. S., Barnes, R. A., and McClain, C. R.: SeaWiFS long-term solar diffuser reflectance and sensor noise analyses, *Applied*
455 *optics*, 46, 762–773, 2007.

456 Eplee Jr, R. E., Sun, J.-Q., Meister, G., Patt, F. S., Xiong, X., and McClain, C. R.: Cross calibration of SeaWiFS and MODIS using on-orbit
457 observations of the Moon, *Applied Optics*, 50, 120–133, 2011.

458 Formenti, P., Andreae, M., Lange, L., Roberts, G., Cafmeyer, J., Rajta, I., Maenhaut, W., Holben, B., Artaxo, P., and Lelieveld, J.: Saharan
459 dust in Brazil and Suriname during the Large-Scale Biosphere-Atmosphere Experiment in Amazonia (LBA)-Cooperative LBA Regional
460 Experiment (CLAIRE) in March 1998, *Journal of Geophysical Research: Atmospheres*, 106, 14 919–14 934, 2001.

461 Formenti, P., Rajot, J. L., Desboeufs, K., Caquineau, S., Chevaillier, S., Nava, S., Gaudichet, A., Journet, E., Triquet, S., Alfaro, S., et al.:
462 Regional variability of the composition of mineral dust from western Africa: Results from the AMMA SOP0/DABEX and DODO field
463 campaigns, *Journal of Geophysical Research: Atmospheres*, 113, 2008.

464 Franz, B. A., Bailey, S. W., Werdell, P. J., and McClain, C. R.: Sensor-independent approach to the vicarious calibration of satellite ocean
465 color radiometry, *Applied optics*, 46, 5068–5082, 2007.

466 Friese, C. A., van der Does, M., Merkel, U., Iversen, M. H., Fischer, G., and Stuut, J.-B. W.: Environmental factors controlling the seasonal
467 variability in particle size distribution of modern Saharan dust deposited off Cape Blanc, *Aeolian Research*, 22, 165–179, 2016.

468 Gamo, M.: Thickness of the dry convection and large-scale subsidence above deserts, *Boundary-Layer Meteorology*, 79, 265–278, 1996.

469 Ganor, E. and Mamane, Y.: Transport of Saharan dust across the eastern Mediterranean, *Atmospheric Environment (1967)*, 16, 581–587,
470 1982.

471 Ganor, E., Osetinsky, I., Stupp, A., and Alpert, P.: Increasing trend of African dust, over 49 years, in the eastern Mediterranean, *Journal of*
472 *Geophysical research: atmospheres*, 115, 2010.

473 Generoso, S., Bey, I., Labonne, M., and Bréon, F.-M.: Aerosol vertical distribution in dust outflow over the Atlantic: Comparisons between
474 GEOS-Chem and Cloud-aerosol Lidar and Infrared Pathfinder Satellite Observation (CALIPSO), *Journal of Geophysical Research: At-*
475 *mospheres*, 113, 2008.

476 Griffin, D. W.: Atmospheric movement of microorganisms in clouds of desert dust and implications for human health, *Clinical microbiology*
477 *reviews*, 20, 459–477, 2007.

478 Heese, B. and Wiegner, M.: Vertical aerosol profiles from Raman polarization lidar observations during the dry season AMMA field cam-
479 paign, *Journal of Geophysical Research: Atmospheres*, 113, 2008.

480 Hervo, M.: Etude des propriétés optiques et radiatives des aérosols en atmosphère réelle: Impact de l'hygroscopicité, Ph.D. thesis, Université
481 Blaise Pascal-Clermont-Ferrand II, 2013.

482 Highwood, E. J., Haywood, J. M., Silverstone, M. D., Newman, S. M., and Taylor, J. P.: Radiative properties and direct effect of Saharan dust
483 measured by the C-130 aircraft during Saharan Dust Experiment (SHADE): 2. Terrestrial spectrum, *Journal of Geophysical Research:*
484 *Atmospheres*, 108, 2003.

485 Holben, B., Tanre, D., Smirnov, A., Eck, T., Slutsker, I., Abuhassan, N., Newcomb, W., Schafer, J., Chatenet, B., Lavenu, F., et al.: An
486 emerging ground-based aerosol climatology: Aerosol optical depth from AERONET, *Journal of Geophysical Research: Atmospheres*,
487 106, 12 067–12 097, 2001.

488 Holben, B. N., Eck, T., Slutsker, I., Tanre, D., Buis, J., Setzer, A., Vermote, E., Reagan, J. A., Kaufman, Y., Nakajima, T., et al.:
489 AERONET—A federated instrument network and data archive for aerosol characterization, *Remote sensing of environment*, 66, 1–16,
490 1998.

491 Hourdin, F., Gueye, M., Diallo, B., Dufresne, J.-L., Escribano, J., Menut, L., Marticoréna, B., Siour, G., and Guichard, F.: Parameterization
492 of convective transport in the boundary layer and its impact on the representation of the diurnal cycle of wind and dust emissions,
493 *Atmospheric Chemistry and Physics*, 15, 6775–6788, 2015.

494 Howell, S., Clarke, A., Shinzuka, Y., Kapustin, V., McNaughton, C., Huebert, B., Doherty, S., and Anderson, T.: Influence of relative
495 humidity upon pollution and dust during ACE-Asia: Size distributions and implications for optical properties, *Journal of Geophysical*
496 *Research: Atmospheres*, 111, 2006.

497 Hsu, N., Gautam, R., Sayer, A., Bettenhausen, C., Li, C., Jeong, M., Tsay, S., and Holben, B.: Global and regional trends of aerosol optical
498 depth over land and ocean using SeaWiFS measurements from 1997 to 2010, 2012.

499 Hsu, N. C., Tsay, S.-C., King, M. D., and Herman, J. R.: Aerosol properties over bright-reflecting source regions, *IEEE Transactions on*
500 *Geoscience and Remote Sensing*, 42, 557–569, 2004.

501 Huneus, N., Schulz, M., Balkanski, Y., Griesfeller, J., Prospero, J., Kinne, S., Bauer, S., Boucher, O., Chin, M., Dentener, F., et al.: Global
502 dust model intercomparison in AeroCom phase I, *Atmospheric Chemistry and Physics*, 11, 2011.

503 Hunt, W. H., Winker, D. M., Vaughan, M. A., Powell, K. A., Lucker, P. L., and Weimer, C.: CALIPSO lidar description and performance
504 assessment, *Journal of Atmospheric and Oceanic Technology*, 26, 1214–1228, 2009.

505 Ialongo, I., Buchard, V., Brogniez, C., Casale, G., and Siani, A.: Aerosol Single Scattering Albedo retrieval in the UV range: an application
506 to OMI satellite validation, *Atmospheric Chemistry and Physics*, 10, 331–340, 2010.

507 Israelevich, P., Ganor, E., Levin, Z., and Joseph, J.: Annual variations of physical properties of desert dust over Israel, *Journal of Geophysical*
508 *Research: Atmospheres*, 108, 2003.

509 Jamet, C., Moulin, C., and Thiria, S.: Monitoring aerosol optical properties over the Mediterranean from SeaWiFS images using a neural
510 network inversion, *Geophysical Research Letters*, 31, 2004.

511 Jethva, H., Torres, O., and Ahn, C.: Global assessment of OMI aerosol single-scattering albedo using ground-based AERONET inversion,
512 *Journal of Geophysical Research: Atmospheres*, 119, 9020–9040, 2014.

513 Jickells, T., An, Z., Andersen, K. K., Baker, A., Bergametti, G., Brooks, N., Cao, J., Boyd, P., Duce, R., Hunter, K., et al.: Global iron
514 connections between desert dust, ocean biogeochemistry, and climate, *science*, 308, 67–71, 2005.

515 Johnson, B. and Osborne, S.: Physical and optical properties of mineral dust aerosol measured by aircraft during the GERBILS campaign,
516 *Quarterly Journal of the Royal Meteorological Society*, 137, 1117–1130, 2011.

517 Johnson, B., Osborne, S., Haywood, J., and Harrison, M.: Aircraft measurements of biomass burning aerosol over West Africa during
518 DABEX, *Journal of Geophysical Research: Atmospheres*, 113, 2008.

519 Joseph, M.: Long-term measurements of the transport of African mineral dust to the southeastern United States: Implications for regional air
520 quality, 1999.

521 Karyampudi, V. M., Palm, S. P., Reagen, J. A., Fang, H., et al.: Validation of the Saharan dust plume conceptual model using lidar, Meteosat,
522 and ECMWF data, *Bulletin of the American Meteorological Society*, 80, 1045, 1999.

523 Kaufman, Y., Koren, I., Remer, L., Tanré, D., Ginoux, P., and Fan, S.: Dust transport and deposition observed from the Terra-Moderate
524 Resolution Imaging Spectroradiometer (MODIS) spacecraft over the Atlantic Ocean, *Journal of Geophysical Research: Atmospheres*,
525 110, 2005.

526 Lafore, J.-P., Flamant, C., Guichard, F., Parker, D., Bouniol, D., Fink, A., Giraud, V., Gosset, M., Hall, N., Höller, H., et al.: Progress in
527 understanding of weather systems in West Africa, *Atmospheric Science Letters*, 12, 7–12, 2011.

528 Laurent, B., Marticorena, B., Bergametti, G., Léon, J., and Mahowald, N.: Modeling mineral dust emissions from the Sahara desert using
529 new surface properties and soil database, *Journal of Geophysical Research: Atmospheres*, 113, 2008.

530 Lavaysse, C., Flamant, C., Janicot, S., Parker, D., Lafore, J.-P., Sultan, B., and Pelon, J.: Seasonal evolution of the West African heat low: a
531 climatological perspective, *Climate Dynamics*, 33, 313–330, 2009.

532 Léon, J.-F., Derimian, Y., Chiappello, I., Tanré, D., Podvin, T., Chatenet, B., Diallo, A., and Deroo, C.: Aerosol vertical distribution and optical
533 properties over M’Bour (16.96 W; 14.39 N), Senegal from 2006 to 2008, *Atmospheric Chemistry and Physics*, 9, 9249–9261, 2009.

534 Levelt, P. F., van den Oord, G. H., Dobber, M. R., Malkki, A., Visser, H., de Vries, J., Stammes, P., Lundell, J. O., and Saari, H.: The ozone
535 monitoring instrument, *IEEE Transactions on geoscience and remote sensing*, 44, 1093–1101, 2006.

536 Liu, D., Wang, Z., Liu, Z., Winker, D., and Trepte, C.: A height resolved global view of dust aerosols from the first year CALIPSO lidar
537 measurements, *Journal of Geophysical Research: Atmospheres*, 113, 2008.

538 Liu, D., Wang, Y., Wang, Z., and Zhou, J.: The three-dimensional structure of transatlantic African dust transport: a new perspective from
539 CALIPSO LIDAR measurements, *Advances in Meteorology*, 2012, 2012.

540 Liu, Z., Omar, A., Hu, Y., Vaughan, M., Winker, D., Poole, L., and Kovacs, T.: CALIOP algorithm theoretical basis document. Part 3: Scene
541 classification algorithms, NASA-CNES document PC-SCI-203, 2005.

542 Mahowald, N., Albani, S., Kok, J. F., Engelstaeder, S., Scanza, R., Ward, D. S., and Flanner, M. G.: The size distribution of desert dust
543 aerosols and its impact on the Earth system, *Aeolian Research*, 15, 53–71, 2014.

544 Mahowald, N. M., Engelstaedter, S., Luo, C., Sealy, A., Artaxo, P., Benitez-Nelson, C., Bonnet, S., Chen, Y., Chuang, P. Y., Cohen, D. D.,
545 et al.: Atmospheric Iron Deposition: Global Distribution, Variability, and Human Perturbations*, *Annual Review of Marine Science*, 1,
546 245–278, 2009.

547 Malavelle, F.: Effets direct et semi-direct des aérosols en Afrique de l’ouest pendant la saison sèche, Ph.D. thesis, Université Paul Sabatier-
548 Toulouse III, 2011.

549 Marticorena, B., Chatenet, B., Rajot, J.-L., Traoré, S., Coulibaly, M., Diallo, A., Koné, I., Maman, A., NDiaye, T., and Zakou, A.: Temporal
550 variability of mineral dust concentrations over West Africa: analyses of a pluriannual monitoring from the AMMA Sahelian Dust Transect,
551 *Atmospheric Chemistry and Physics*, 10, 8899–8915, 2010.

552 Martin, J. H.: Iron as a limiting factor in oceanic productivity, in: *Primary productivity and biogeochemical cycles in the sea*, pp. 123–137,
553 Springer, 1992.

554 Martiny, N. and Chiapello, I.: Assessments for the impact of mineral dust on the meningitis incidence in West Africa, *Atmospheric Environ-
555 ment*, 70, 245–253, 2013.

556 McConnell, C., Highwood, E., Coe, H., Formenti, P., Anderson, B., Osborne, S., Nava, S., Desboeufs, K., Chen, G., and Harrison, M.:
557 Seasonal variations of the physical and optical characteristics of Saharan dust: Results from the Dust Outflow and Deposition to the Ocean
558 (DODO) experiment, *Journal of Geophysical Research: Atmospheres*, 113, 2008.

559 Messenger, C., Parker, D. J., Reitebuch, O., Agustí-Panareda, A., Taylor, C. M., and Cuesta, J.: Structure and dynamics of the Saharan
560 atmospheric boundary layer during the West African monsoon onset: Observations and analyses from the research flights of 14 and 17
561 July 2006, *Quarterly Journal of the Royal Meteorological Society*, 136, 107–124, 2010.

562 Mielonen, T., Arola, A., Komppula, M., Kukkonen, J., Koskinen, J., de Leeuw, G., and Lehtinen, K.: Comparison of CALIOP level 2 aerosol
563 subtypes to aerosol types derived from AERONET inversion data, *Geophysical Research Letters*, 36, 2009.

564 Mills, M. M., Ridame, C., Davey, M., La Roche, J., and Geider, R. J.: Iron and phosphorus co-limit nitrogen fixation in the eastern tropical
565 North Atlantic, *Nature*, 429, 292–294, 2004.

566 Mokhtari, M.: Amélioration de la prise en compte des aérosols terrigènes dans les modèles atmosphériques à moyenne échelle, Ph.D. thesis,
567 Université de Toulouse, Université Toulouse III-Paul Sabatier, 2012.

568 Mortier, A., Goloub, P., Derimian, Y., Tanré, D., Podvin, T., Blarel, L., Deroo, C., Marticorena, B., Diallo, A., and Ndiaye, T.: Climatology
569 of aerosol properties and clear-sky shortwave radiative effects using Lidar and Sun photometer observations in the Dakar site, *Journal of
570 Geophysical Research: Atmospheres*, 2016.

571 Moulin, C.: Transport atmosphérique des poussières africaines sur la Méditerranée et l’Atlantique: climatologie satellitale à partir des images
572 Météosat VIS(1983-1994) et relations avec le climat, Ph.D. thesis, 1997.

573 Omar, A. H., Winker, D. M., Vaughan, M. A., Hu, Y., Trepte, C. R., Ferrare, R. A., Lee, K.-P., Hostetler, C. A., Kittaka, C., Rogers, R. R.,
574 et al.: The CALIPSO automated aerosol classification and lidar ratio selection algorithm, *Journal of Atmospheric and Oceanic Technology*,
575 26, 1994–2014, 2009.

576 Ozer, P.: Les lithométéores en région sahélienne: un indicateur climatique de la désertification, Ph.D. thesis, Université de Liège Faculté des
577 sciences Liège Belgique, Liège, Belgique, 2000.

578 Petzold, A., Veira, A., Mund, S., Esselborn, M., Kiemle, C., Weinzierl, B., Hamburger, T., Ehret, G., Lieke, K., and Kandler, K.: Mixing of
579 mineral dust with urban pollution aerosol over Dakar (Senegal): impact on dust physico-chemical and radiative properties, *Tellus B*, 63,
580 619–634, 2011.

581 Prospero, J., Glaccum, R., and Nees, R.: Atmospheric transport of soil dust from Africa to South America, *Nature*, 289, 570–572, 1981.

582 Prospero, J. M., Blades, E., Mathison, G., and Naidu, R.: Interhemispheric transport of viable fungi and bacteria from Africa to the Caribbean
583 with soil dust, *Aerobiologia*, 21, 1–19, 2005.

584 Ramanathan, V., Crutzen, P., Kiehl, J., and Rosenfeld, D.: Aerosols, climate, and the hydrological cycle, *science*, 294, 2119–2124, 2001.

585 Reid, J. S., Westphal, D. L., Livingston, J. M., Savoie, D. L., Maring, H. B., Jonsson, H. H., Eleuterio, D. P., Kinney, J. E., and Reid, E. A.:
586 Dust vertical distribution in the Caribbean during the Puerto Rico Dust Experiment, *Geophysical research letters*, 29, 2002.

587 Ridley, D., Heald, C., and Ford, B.: North African dust export and deposition: A satellite and model perspective, *Journal of Geophysical*
588 *Research: Atmospheres*, 117, 2012.

589 Ryder, C., Highwood, E., Lai, T., Sodemann, H., and Marsham, J.: Impact of atmospheric transport on the evolution of microphysical and
590 optical properties of Saharan dust, *Geophysical Research Letters*, 40, 2433–2438, 2013.

591 Sayer, A., Hsu, N., Bettenhausen, C., Ahmad, Z., Holben, B., Smirnov, A., Thomas, G., and Zhang, J.: SeaWiFS Ocean Aerosol Retrieval
592 (SOAR): Algorithm, validation, and comparison with other data sets, *Journal of Geophysical Research: Atmospheres*, 117, 2012.

593 Schepanski, K., Tegen, I., Laurent, B., Heinold, B., and Macke, A.: A new Saharan dust source activation frequency map derived from
594 MSG-SEVIRI IR-channels, *Geophysical Research Letters*, 34, 2007.

595 Schepanski, K., Tegen, I., and Macke, A.: Saharan dust transport and deposition towards the tropical northern Atlantic, *Atmos. Chem. Phys*,
596 9, 1173–1189, 2009a.

597 Schepanski, K., Tegen, I., Todd, M., Heinold, B., Bönisch, G., Laurent, B., and Macke, A.: Meteorological processes forcing Saharan dust
598 emission inferred from MSG-SEVIRI observations of subdaily dust source activation and numerical models, *Journal of Geophysical*
599 *Research: Atmospheres*, 114, 2009b.

600 Schepanski, K., Tegen, I., and Macke, A.: Comparison of satellite based observations of Saharan dust source areas, *Remote Sensing of*
601 *Environment*, 123, 90–97, 2012.

602 Shao, Y.: *Physics and modelling of wind erosion (atmospheric and oceanographic sciences library)*, 2000.

603 Slutsker, I. and Kinne, S.: Wavelength dependence of the optical depth of biomass burning, urban, and desert dust aerosols, *J Geophys Res*,
604 104, 00 093–5, 1999.

605 Sokolik, I. N. and Toon, O. B.: Incorporation of mineralogical composition into models of the radiative properties of mineral aerosol from
606 UV to IR wavelengths, *Journal of Geophysical Research*, 104, 9423–9444, 1999.

607 Solomon, S.: *Climate change 2007-the physical science basis: Working group I contribution to the fourth assessment report of the IPCC*,
608 vol. 4, Cambridge University Press, 2007.

609 Stith, J., Ramanathan, V., Cooper, W., Roberts, G., DeMott, P., Carmichael, G., Hatch, C., Adhikary, B., Twohy, C., Rogers, D., et al.: An
610 overview of aircraft observations from the Pacific Dust Experiment campaign, *Journal of Geophysical Research: Atmospheres*, 114, 2009.

611 Swap, R., Garstang, M., Greco, S., Talbot, R., and Kållberg, P.: Saharan dust in the Amazon Basin, *Tellus B*, 44, 133–149, 1992.

612 Taghavi, F. and Asadi, A.: The Persian Gulf 12th April 2007 dust storm: observation and model analysis, in: EUMETSAT Meteorological
613 Satellite Conference, Darmstadt, Germany, pp. 8–12, 2008.

614 Tanaka, T. Y., Kurosaki, Y., Chiba, M., Matsumura, T., Nagai, T., Yamazaki, A., Uchiyama, A., Tsunematsu, N., and Kai, K.: Possible
615 transcontinental dust transport from North Africa and the Middle East to East Asia, *Atmospheric Environment*, 39, 3901–3909, 2005.

616 Tegen, I., Schepanski, K., and Heinold, B.: Comparing two years of Saharan dust source activation obtained by regional modelling and
617 satellite observations, *Atmospheric Chemistry and Physics*, 13, 2381–2390, 2013.

618 Teller, A. and Levin, Z.: The effects of aerosols on precipitation and dimensions of subtropical clouds: a sensitivity study using a numerical
619 cloud model, *Atmospheric Chemistry and Physics*, 6, 67–80, 2006.

620 Thomson, M. C., Molesworth, A. M., Djingarey, M. H., Yameogo, K., Belanger, F., and Cuevas, L. E.: Potential of environmental models to
621 predict meningitis epidemics in Africa, *Tropical Medicine & International Health*, 11, 781–788, 2006.

622 Tsamalis, C., Chédin, A., Pelon, J., and Capelle, V.: The seasonal vertical distribution of the Saharan Air Layer and its modulation by the
623 wind, *Atmospheric Chemistry and Physics*, 13, 11 235–11 257, 2013.

624 Tulet, P., Mallet, M., Pont, V., Pelon, J., and Boone, A.: The 7–13 March 2006 dust storm over West Africa: Generation, transport, and
625 vertical stratification, *Journal of Geophysical Research: Atmospheres*, 113, 2008.

626 Vuolo, M. R., Chepfer, H., Menut, L., and Cesana, G.: Comparison of mineral dust layers vertical structures modeled with CHIMERE-DUST
627 and observed with the CALIOP lidar, *Journal of Geophysical Research: Atmospheres*, 114, 2009.

628 Wagener, T.: Le fer à l’interface océan-atmosphère: Flux et processus de dissolution dans l’eau de mer., Ph.D. thesis, Université de la
629 Méditerranée-Aix-Marseille II, 2008.

630 Wang, M., Bailey, S., Pietras, C., McClain, C., and Riley, T.: SeaWiFS aerosol optical thickness matchup analyses, The Sea-WiFS Postlaunch
631 Technical Report Series, 10, 39–44, 2000.

632 Weinzierl, B., Ansmann, A., Prospero, J., Althausen, D., Benker, N., Chouza, F., Dollner, M., Farrell, D., Fomba, W., Freudenthaler, V., et al.:
633 The Saharan Aerosol Long-range Transport and Aerosol-Cloud-Interaction Experiment (SALTRACE): overview and selected highlights,
634 *Bulletin of the American Meteorological Society*, 2016.

635 Winker, D.: Accounting for multiple scattering in retrievals from space lidar, in: *Proc. of SPIE Vol.*, vol. 5059, p. 129, 2003.

636 Winker, D. M., Hostetler, C., Vaughan, M., and Omar, A.: CALIOP Algorithm Theoretical Basis Document, Part 1: CALIOP Instrument,
637 and Algorithms Overview, Release, 2, 29, 2006.

638 Winker, D. M., Hunt, W. H., and McGill, M. J.: Initial performance assessment of CALIOP, *Geophysical Research Letters*, 34, 2007.

639 Wu, M.-L. C., Reale, O., Schubert, S. D., Suarez, M. J., Koster, R. D., and Pegion, P. J.: African easterly jet: structure and maintenance,
640 *Journal of Climate*, 22, 4459–4480, 2009.

641 Yang, W., Marshak, A., Várnai, T., Kalashnikova, O. V., and Kostinski, A. B.: CALIPSO observations of transatlantic dust: vertical stratifi-
642 cation and effect of clouds, *Atmospheric Chemistry and Physics*, 12, 11 339–11 354, 2012.

643 Yu, H., Chin, M., Winker, D. M., Omar, A. H., Liu, Z., Kittaka, C., and Diehl, T.: Global view of aerosol vertical distributions from CALIPSO
644 lidar measurements and GOCART simulations: Regional and seasonal variations, *Journal of Geophysical Research: Atmospheres*, 115,
645 2010.

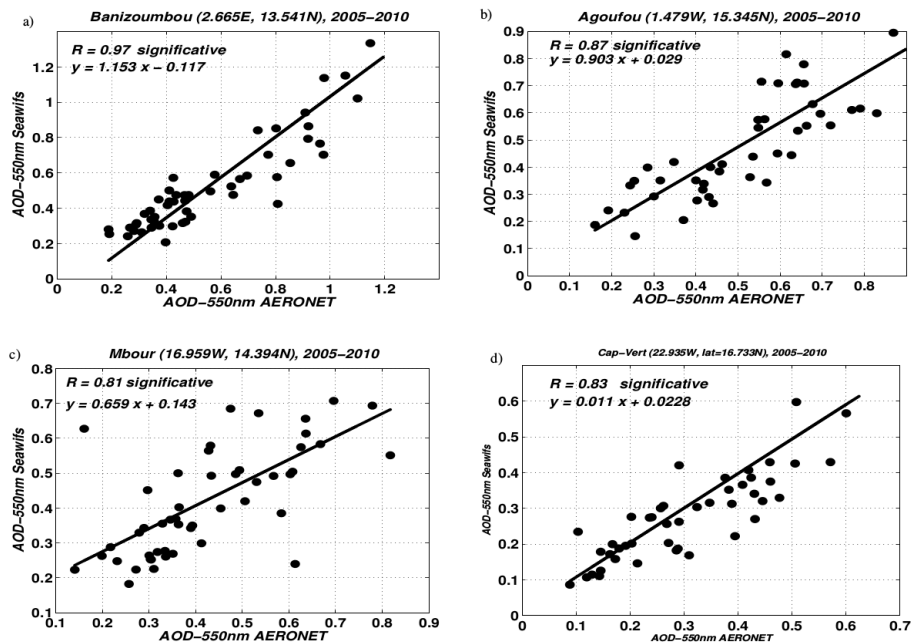


Figure 1. Comparison of monthly mean aerosol optical depth (AOD) between SeaWiFS (550 nm) and ground measurements from AERONET (675 nm) from January 2005 to December 2010. This comparison is done at the following stations : a) Banizoumbou (53 points), b) Agoufou (47 points), c) M'bour (50 points) and d) Cape verde (47 points). The red solid line represents the regression between both dataset

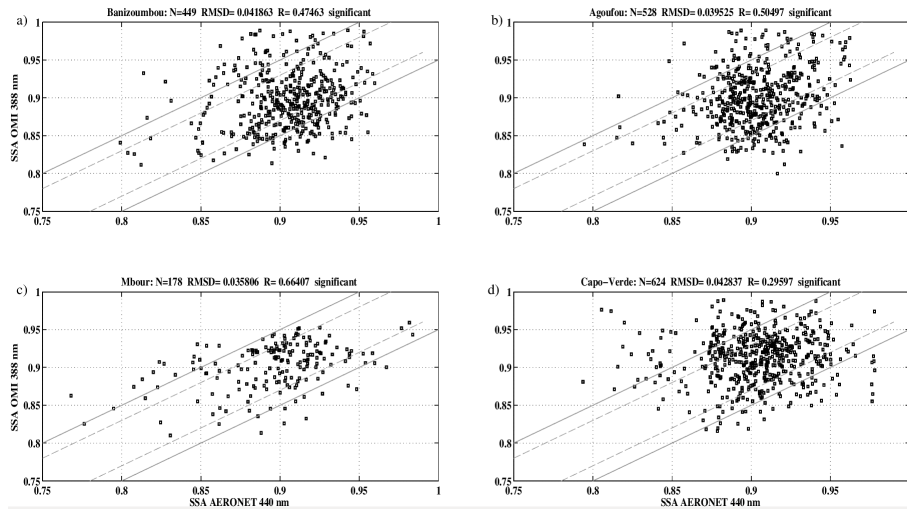


Figure 2. OMAERUV SSA at 388 nm wavelength as a function of AERONET SSA at 440 nm at a) Banizoumbou (2.66°E,13.54°N; 449 retrievals); b) Agoufou (1.47°W, 15.34°N; 528 retrievals); c) Mbour (16.95°W, 14.39°N; 178 retrievals) and d) Capo Verde (22.93°W, 16.73°N; 624 retrievals). The solid lines indicate the domain where the two retrievals agree with each other within 0.03 and the dashed lines indicate agreement within 0.05.

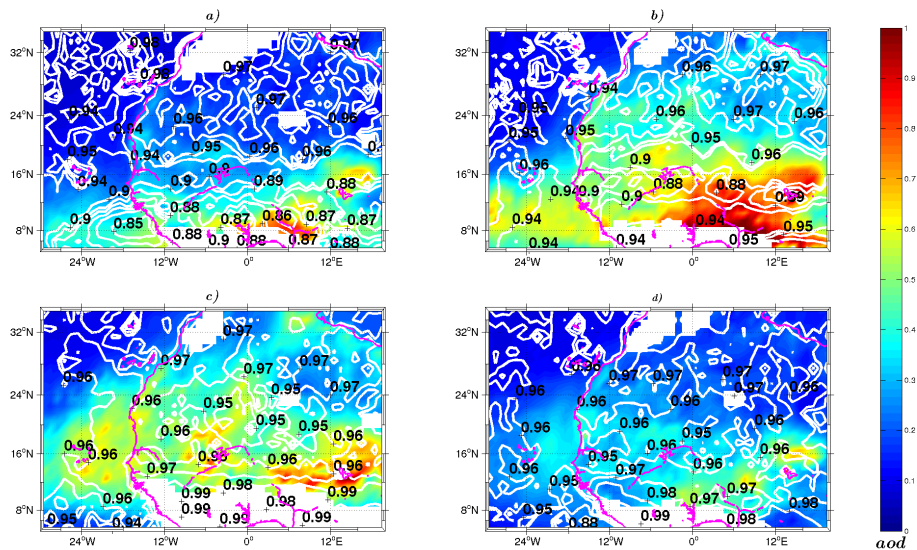


Figure 3. Seasonal distribution of aerosol optical depth (average between 2005 and 2010) at 550 nm wavelength (colours) from SeaWiFS for a) DJF; b) MAM; c) JJA and d) SON. SSA from OMI is superimposed with white contour lines.

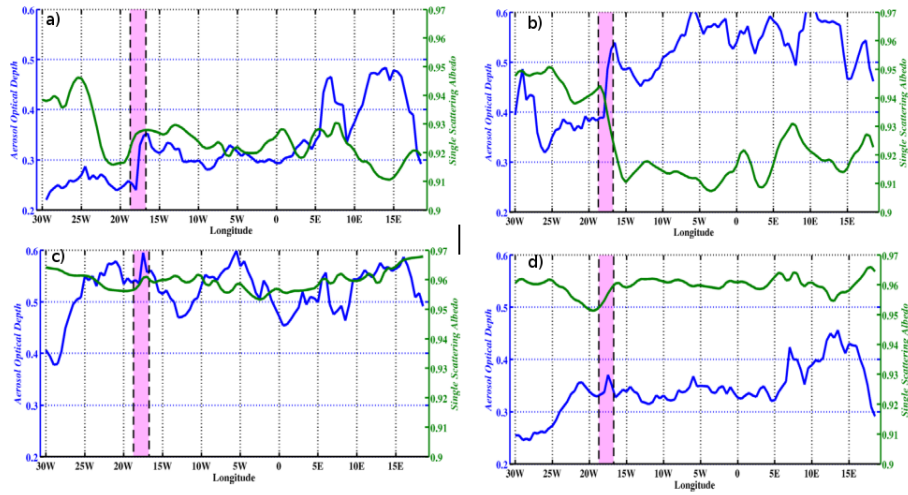


Figure 4. Seasonal SeaWiFS AOD at 550 nm (bleu), Aura/OMI SSA (green) zonally averaged between 12° and 21°N and from 2005 to 2010: a) DJF; b) MAM; c) JJA; and d) SON. The black dashed lines indicate the continent-ocean transition for the latitude range 12°-21°N.

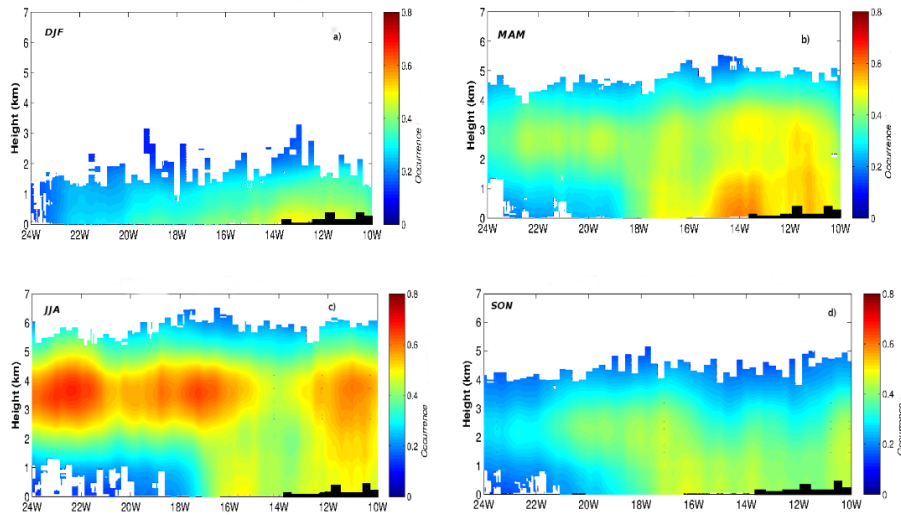


Figure 5. CALIOP daytime seasonal vertical distribution of the frequency of mineral dust aerosol occurrence zonally averaged between 12° and 21°N over the period 2007-2013: a) DJF; b) MAM; c) JJA; and d) SON.

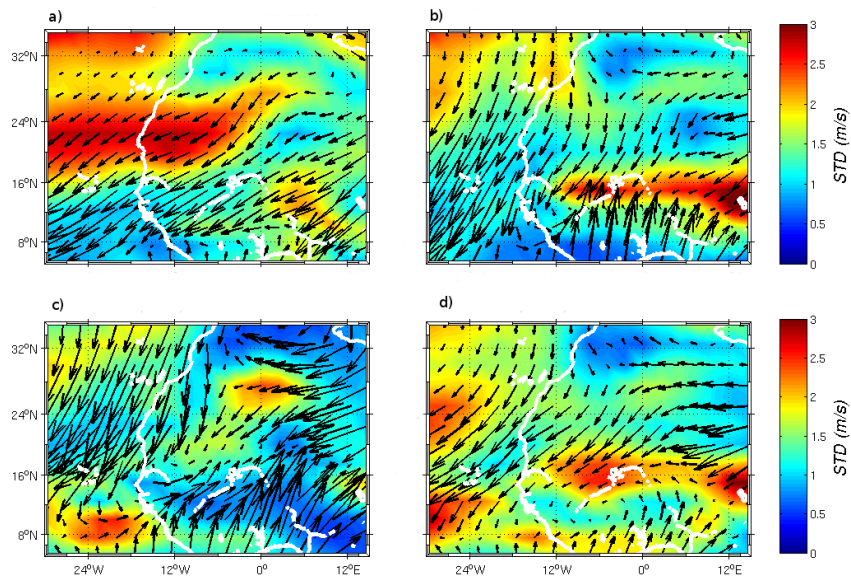


Figure 6. Seasonal mean zonal wind field at 925 hPa over West Africa from NCEP Reanalysis between 2000 and 2012: a) DJF; b) MAM; c) JJA; and d) SON. The vectors show wind direction while colors indicate the standard deviation of wind velocity ($\text{m}\cdot\text{s}^{-1}$).

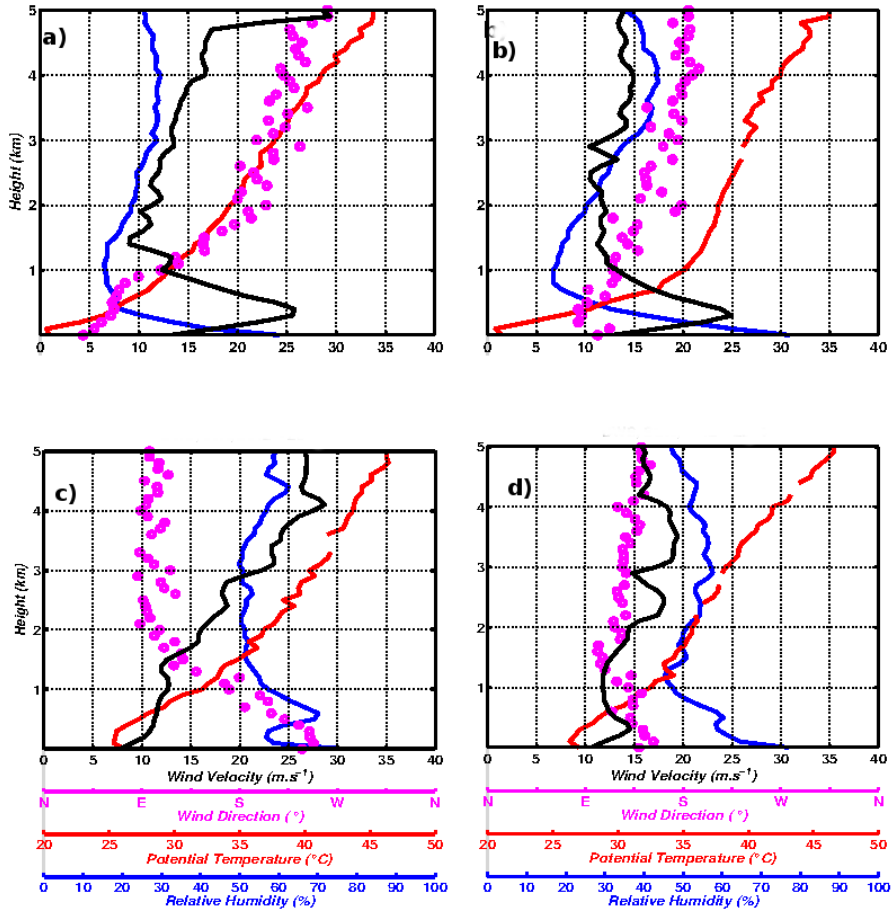


Figure 7. Mean seasonal vertical profiles of wind velocity (black line), wind direction (pink dots), potential temperature (red line) and relative humidity (blue line) at Dakar weather station (14.73°N, 17.51°W) for a) DJF; b) MAM; c) JJA; and d) SON. Observations correspond to weather balloon launched daily at 12UTC for years 2012 to 2014.